

GLOBAL MODELLING WITHIN THE CSIRO
DIVISION OF ATMOSPHERIC RESEARCH

B.G. HUNT

1. INTRODUCTION

Numerical modelling is now used very extensively in science and technology to investigate an enormous range of problems, from biology to aerodynamics. One of the most active areas of modelling has always been the climatic sciences. Currently very complex models have been developed for the atmosphere and oceans, which are being increasingly applied to critical problems such as long range weather forecasting, studies of the greenhouse effect, drought research and prediction, and problems associated with atmospheric composition. Apart from the practical utility of such research, a principal reason for numerical modelling developing so rapidly in the climatic area is the existence of well-defined mathematical equations, which control the large scale motions in the atmosphere and oceans. These equations can be manipulated into forms which permit them to be solved on computers, thereby allowing climatic simulations and predictions to be made. Of course, the accuracy of the models is limited in practice by our lack of knowledge about many physical processes in the atmosphere and particularly the oceans. Problem areas include clouds and their interactions, exchange processes between the atmosphere and oceans, and the mechanisms governing the changes in many oceanic properties.

The formulation and description of such models will not be considered here, but relevant details can be obtained from GARP[1] or CHANG[2].

2. CLIMATIC MODELS IN USE AT THE CSIRO DIVISION OF ATMOSPHERIC RESEARCH

Three models are currently in use, two of these models are intended for general climatic studies, the third is more specifically designed for middle atmospheric simulations.

The most actively used model is one designed in this Division with 4-vertical layers, which has been successfully applied to problems of climatic variability, greenhouse effect studies and simulation and prediction of drought. This model includes most important climatic features such as land-sea contrast, mountains, sea ice and snow cover, calculation of the cloud amounts and diurnal and seasonal variability. Fixed sea surface temperature (SST) defined from climatology are used in many of the experiments. The basic atmospheric fields of north-south wind, east-west wind, temperature, humidity and pressure are computed at half-hourly intervals. The model uses a spectral formulation to represent geographical variability of these fields with 21 wave numbers in the east-west direction. The vertical formulation uses the predictive equations in the flux form, which guarantees global conservation of mass, momentum, energy and humidity. This is the only spectral model in the world which currently has this fundamental conservative property.

The other general climatic model is that developed at the Bureau of Meteorology Research Centre, and principally differs from the previous model by having 9-vertical layers and omitting the conservative property noted above. This model has not been used as extensively as the 4-layer model, as a number of its physical processes have still to be fine tuned. It is intended

to replace this model within the Division of Atmospheric Research by reformulating the 4-layer model to 9-layers.

The middle atmospheric model developed within the Division of Atmospheric Research has 54-layers extending from the surface to 100 km. Because of the complexity of the meteorological processes which occur in the middle atmosphere this model currently omits mountains and the hydrologic cycle. Because of limitations on super computer time, the model has also only been run in the fixed January mode so far. The model is formulated somewhat differently to the above two models, as it has a finite difference grid in a single north-south plane, with east-west variations represented by a Fourier series of 15 wave numbers. The model has been consistently developed over a period of some years, and now produces a fairly satisfactory simulation of many middle atmospheric features.

3. MODEL RESULTS

(a) 4-layer model

As a broad indication of the model's general capability of simulating the current climate Fig. 1 compares the observed and computed climatological surface pressure distributions for January. Apart from some problems at very high latitudes, where traditionally models have experienced difficulties, the overall agreement is rather satisfactory as regards intensity and location of the major features. The one exception to this situation is the somewhat distorted Siberian high in the model, which can be attributed to the problems of representing orography in models of the horizontal resolution used here. Over the Australian region the agreement between the model and observation is very good. A range of other climatic variables

are also available for comparison, which brevity precludes from being presented here. Overall, the agreement between model and observation is satisfactory, with the exception of rainfall. An adequate simulation of rainfall is always difficult, and, while the general characteristics are reasonably well produced, specific problems occur such as excessive extension of monsoonal rainfall southeastwards over Australia.

As part of the drought research programme being undertaken with this model, extensive studies of the hydrologic cycle have been made. One component of this cycle, soil moisture, is shown in Fig.2, from Gordon and Hunt [3], from an earlier version of the model when it had only 2-vertical levels. This figure illustrates the ability of the model to simulate a wide range of different climatic regimes in different geographical areas, and also its capacity to reproduce a considerable degree of interannual variability during the course of a 10-year integration. One particularly interesting feature of this figure is the interannual variability of the soil moisture, and thus the rainfall, over Somalia. Some years with quite marked drought are apparent, and similar characteristics can be observed at some other localities such as Morocco and California. The results in Fig.2 are for individual model gridpoints, and when the analysis was extended to adjacent areas, Hunt and Gordon [4], it was found that such droughts were very local, being essentially confined to single gridpoints. This is an example of "naturally-occurring" drought, which can also be identified in observations in Australia for example, Hunt and Gordon [4]. Such droughts do not have a specific, identifiable precursor mechanism, and arise from the natural variability of the climatic system owing to its inherent

nonlinearity. As such these droughts are unpredictable, but fortunately very localised.

A well-established drought precursor is SST anomalies, with the best known example being the so-called El Nino event which involves a warming of 2-3 Celsius in the central and eastern Pacific Ocean. Idealised, but typical, El Nino SST anomaly patterns are shown in Fig.3. These patterns were used in drought simulation experiments, with the 4-layer model run in a fixed January mode, by superimposing the SST anomalies upon the existing specified SST distribution in the model. One experiment, called run D, involved only the warm anomaly in the central and eastern Pacific, the other, run E, used this anomaly together with the cold anomaly north of Australia. The results of such experiments are compared with a control run in which no SST anomalies were present.

The impact of these anomalies on the rainfall, for specific model gridpoints shown blacked out in Fig.3, is illustrated in Fig.4 by time series plots of accumulating rainfall. The west Australian point, Australia 1 in Fig.4, is outside of the general area of influence of an El Nino and consequently shows relatively little response to the SST anomalies. On the other hand the Australia 2 and Australia 3 points located in the eastern half of the continent experienced very marked drought situations in the D and E runs, thereby illustrating the effectiveness of relatively small SST anomalies in producing droughts. The drought associated with these anomalies actually extended over the eastern half of the continent. As shown in Fig.4(f) a drought was also produced in Venezuela in both the D and E runs. In contrast to these droughts Fig.4(d) and 4(e) show "flood" conditions were produced at the central Pacific and

Peruvian points in Fig.3. These large scale rainfall variations arise from the perturbations induced in the atmospheric circulation patterns over the Pacific basin by the SST anomalies, and are all part of a phenomenon known nowadays as ENSO (El Nino/Southern Oscillation). The rainfall changes shown in Fig.4 agree quite well with composited ENSO observations reported by Ropelewski and Halpert [5].

A simulation of the 1988 US drought has been made with the 4-layer model in a somewhat more elaborate experiment involving multiple runs under seasonally varying conditions. The precursor mechanism used was again SST anomalies in the Pacific Ocean, but in this case the actual observed anomalies reported at monthly intervals were used. A comparison of the rainfall changes experienced in one of these experiments with observed extreme rainfall patterns is given in Fig.5 for May to August. While specific, local differences can be identified between the computed and observed rainfall patterns in individual months, the model simulated the overall drought conditions on the North American continent, as well as a number of the enhanced rainfall episodes. Since considerable potential exists for improving the model and the way the experiments were conducted, even more realistic simulations are possible in the future.

However, a practical problem in drought simulations (and predictions) arises from the sensitivity of the model results to initial conditions. This is illustrated in Fig.5 from Smith and Gordon [6] where results from multiple runs with the 4-layer model using the same El Nino type SST anomaly, but starting from different years of a multiannual control-run, are compared. Monthly rainfall differences from the individual control runs are shown for 5 runs for a model gridpoint in northern

Australia. While 4 of these runs reveal rainfall deficits with a marked drought occurring during the wet season late in the year, one run experienced enhanced rainfall. The implications of this result are that simulations and predictions will require a Monte Carlo approach involving a number of runs for a given situation and compositing of the results. While this requirement compounds the complexity of experiments and increases the computational requirements, it will permit estimates of the likely range of rainfall anomalies and their standard deviations to be calculated. This should result in greater confidence in the results.

Drought prediction experiments are also being conducted with the 4-layer model. These experiments require the SST anomaly precursor to be predicted and then the use of these anomalies in the 4-layer model. The SST anomaly predictions are being performed by Dr Hughes of this Division and Dr Kleeman of the Bureau of Meteorology Research Centre. The test period for these predictions has been selected to be the great El Nino event of 1982. The predictions involve using observed winds to drive an elementary model of the Pacific Ocean basin (30°N to 30°S) for a number of years prior to 1982. At the beginning of 1982 it is assumed that no observational data exist, and a simple atmospheric model is then coupled to the oceanic model and the experiment goes into a predictive phase for an 18-month period. This coupled model outputs SST anomalies at monthly intervals for the Pacific Ocean, which are subsequently used in the 4-layer model. While considerable improvement is needed in the accuracy of the El Nino SST anomalies, the drought predictions performed to date are encouraging in that in some months fairly realistic rainfall perturbations were produced,

and the breaking of the drought in 1983 was also reproduced. A number of specific improvements to the models are planned to enhance its performance in future experiments.

As mentioned earlier the 4-layer model is also being used in greenhouse research and, in fact, the first greenhouse modelling experiment to be carried out in Australia has recently been completed with this model. This experiment involved multi-decadal runs with the model to generate the required climatic distributions and statistics. The details of these runs will not be discussed other than to note that a control run (with 1 x CO₂), as well as a greenhouse run (with 2 x CO₂), is required, as it is the *difference* in these two runs which is of interest. An indication of the response of the model to an instantaneous doubling of CO₂, and the global mean temperature increase of 4°C, is given in Fig.7. This figure indicates a response time of about 10 years exists before the model equilibrates to the changed CO₂ amount.

Preliminary examination of the model results reveals marked climatic changes for 2 x CO₂, particularly at the regional level. For example, large changes occur in the sea ice distribution, with the Arctic sea ice cover virtually disappearing in summer, but returning very rapidly with the onset of winter. Other variables also experience substantial changes, which brevity prevents from being discussed here.

Before presenting some sample results for the Australia region based on long-term averages it is interesting to examine the year-to-year variability of results within such averages. Figure 8 shows the surface temperature differences for a single February of the 2 x CO₂ run from those of the long term average of the 1 x CO₂ run. While the corresponding temperature

differences between the long term averages of both the 2 x CO₂ and 1 x CO₂ runs exhibit global warming, Fig. 8 indicates that individual years can experience both warmings and coolings. This highlights an essential point of greenhouse scenarios: that is there will be quite marked interannual variability within such scenarios, and in some years for some regions noticeably different weather patterns will be experienced from the generally portrayed greenhouse "climate".

The model simulation for January conditions of the surface temperature changes for time averaged results over the Australian region is illustrated in Fig.9. For most of Australia a temperature increase of over 3°C is projected under average greenhouse conditions, with an increase of greater than 5°C for a large part of West Australia. The latter is associated with a general drying out of this region. Examination of the temperature changes for individual years of the greenhouse run revealed temperature increases of over 10°C in West Australia in some years! In winter a more uniform warming of about 4°C was obtained over Australia as a whole for time averaged conditions. Associated with these temperature increases was an overall decrease in surface pressure over Australia of between 1 and 2mb, with corresponding increases in pressure south of the continent.

A final result from the greenhouse experiment is given in Fig.10 where the January position of the so-called monsoonal shear line is shown. This shear line separates west winds to the north and east winds to the south, and approximately delineates the southwards extension of the monsoonal rains. The control run results agree quite well with observations. Comparison of the two simulations in Fig.10 suggests that the

location of the shear line would not be expected to move noticeably under greenhouse conditions, hence monsoonal rains and associated mosquito infestations etc should not spread southwards. Since this shear line also acts as the spawning ground for tropical cyclones, this feature should also be unchanged; although the more intense winds in the greenhouse scenario might imply stronger cyclone intensities. The general warming of the oceans around Australia illustrated in Fig.9 does indicate that cyclones should be able to propagate further southwards as the minimum oceanic temperature of 27°C needed to maintain cyclonic activity moves southwards under greenhouse conditions.

(b) 9-layer model

As mentioned above, this model has not been used in the extensive range of experiments described for the 4-layer model, and is currently being replaced by an extension of the latter model to 9 layers. Hence only one example of its performance, concerned with its simulation of clouds, will be considered here.

In general, cloud amount in models is evaluated from the computed relative humidity. The latter in turn depends on the temperature and specific humidity distributions generated in the model. The zonal mean relative humidity for fixed January conditions in the 9-layer model is shown in Fig.11. The general characteristics of high values in middle latitudes, and especially the tropics, and low values in the arid zones are reproduced by the model. The resulting computed cloud amounts are given in Fig.12(a) and observed values in Fig.12(b). While the overall distributions of the two data sets are similar,

differences are apparent at some latitudes. Geographical plots normally show even more obvious differences in specific regions.

These results highlight a problem currently existing in all models, and underlines the difficulty of computing cloud properties in models which, of necessity, lack the fine scale to resolve the majority of the physical processes involved in the generation of clouds in the actual atmosphere. This situation is expected to be resolved gradually as models include finer scales as computer power increases, and also as a better understanding of the mechanisms operating in the atmosphere is obtained.

(c) 54-layer model

This model has undergone a consistent development programme over a number of years. Because it was the first general circulation model to extend up to 100 km a number of unique problems had to be resolved. The development of the model is illustrated in Fig.13 where the systematic improvement in the mean zonal wind distribution is illustrated. The earliest version of the model, Hunt [7], excluded the diurnal variation of the sun, and gravity wave drag which acts to decelerate the atmospheric flow, particularly above 50 km, see Fig.13(a). The next version of the model included these phenomenon, Hunt [8], with a consequent improvement in the agreement of the model zonal wind with observation, Fig.13(b). The current version of the model, Hunt [9], has an improved gravity wave formulation and radiative scheme in the upper layers of the model, Fig.13(c), resulting in further agreement with observation, Fig.13(d).

A considerable number of the model properties have been documented in the above references and other papers. Of

particular interest is the model's ability to simulate the basic tidal characteristics of the atmosphere between 70 and 100 km, where they dominate the flow fields. An example of the geographical and temporal variations of the north-south winds at 77.5 km in the model is given in Fig.14. The winds are simulated at 6 hourly intervals and show a clear westward progression, as observed, with the tides being more pronounced in the southern (summer) hemisphere. An indication of the variations of the tides with height is shown in Fig.15. This displays the temporal variation of the zonal wind over a 7-day period, for a gridpoint in model located in South Australia. High frequency changes can be seen to occur above about 80 km where tidal characteristics are strongest, with a marked reduction in activity at lower levels.

The final figure, Fig.16, illustrates the interaction between vertically propagating internal gravity waves and tides over a 4-day period. As these waves ascend their time variation is increasingly influenced by the tides, first at the diurnal frequency and then at the semidiurnal frequency. The strength of the waves is also attenuated with height as they are absorbed into the background flow, where they have a considerable impact on the energy and momentum of the local atmosphere.

While much further development of this model is necessary, it holds considerable potential for use in studies of atmospheric constituents, particularly ozone photochemistry, and in specialised solar-terrestrial experiments.

4. CONCLUSIONS

The global models developed with the CSIRO Division of Atmospheric Research now permit a wide range of climatic

problems to be investigated. The physical mechanisms incorporated in these models are being systematically improved to enhance the performance of the models; the common origins of the 4-layer and the redesigned 9-layer model will materially assist such enhancements. Certainly the environmental problems associated with the ozone hole, the greenhouse effect, droughts and desertification and climatic variability will ensure the need for these models for many years to come.

Currently a major effort has been committed to coupling the 4- and 9-layer models to general circulation models of the oceans, in order to produce coupled climatic models. Such models are needed for realistic studies of most of the above listed problems. It is also intended to begin the design of a completely new model, which will enable the Division's research programme to be advanced into the next century. This model will be organised to improve coupling processes with the oceans, to represent better the planetary boundary layer, and to permit a more accurate simulation of atmospheric photochemistry up to the stratopause. It will also be more modular in order to permit new physical parameterizations to be tested. Importantly, it will be structured to take advantage of the multi-processing capabilities of future generations of supercomputers. This model should enable Australia to stay at the forefront of climatic studies worldwide.

Acknowledgement. The author would like to thank his colleagues Drs Gordon, Hughes, Ryan, Smith and Watterson for permitting him to present results from their research.

REFERENCES

- [1] GARP (1975). The physical basis of climate and climate modelling. GARP Pub.Ser.No.16, 265pp. (World Meteorological Organization, Geneva).
- [2] CHANG, J. ed. (1977). Methods in Computational Physics, Volume 17. General Circulation Models of the Atmosphere. Academic Press.
- [3] GORDON, H.B. and HUNT, B.G., (1987). Interannual variability of the simulated hydrology in a climatic model - implications for drought. *Climate Dynamics*, 1, 113-130.
- [4] HUNT, B.G. and GORDON, H.B., (1988). The problem of naturally-occurring drought. *Climate Dynamics*, 3, 19-33.
- [5] ROPELEWSKI, C.F. and HALPERT, M.S., (1987). Global and regional scale precipitation patterns associated with the El Nino/Southern Oscillation. *Mon.Wea.Rev.*, 115, 1606-1626.
- [6] SMITH, I.N. and GORDON, H.B., (1990). Numerical simulation of atmospheric anomaly patterns associated with warm Equatorial Pacific SSTs. To be submitted to *Climate Dynamics*.
- [7] HUNT, B.G., (1981). The maintenance of the zonal mean state of the upper atmosphere as represented in a three-dimensional general circulation model extending to 100 km. *J.Atmos.Sci.*, 38, 2172-2186.
- [8] HUNT, B.G., (1986). The impact of gravity wave drag and diurnal variability on the general circulation of the middle atmosphere. *J.Meteor.Soc.Japan*, 64, 1-16.
- [9] HUNT, B.G. (1990). A simulation of the gravity wave characteristics and interactions in a diurnally varying model atmosphere. *J.Meteor.Soc.Japan*, 68, 145-161.

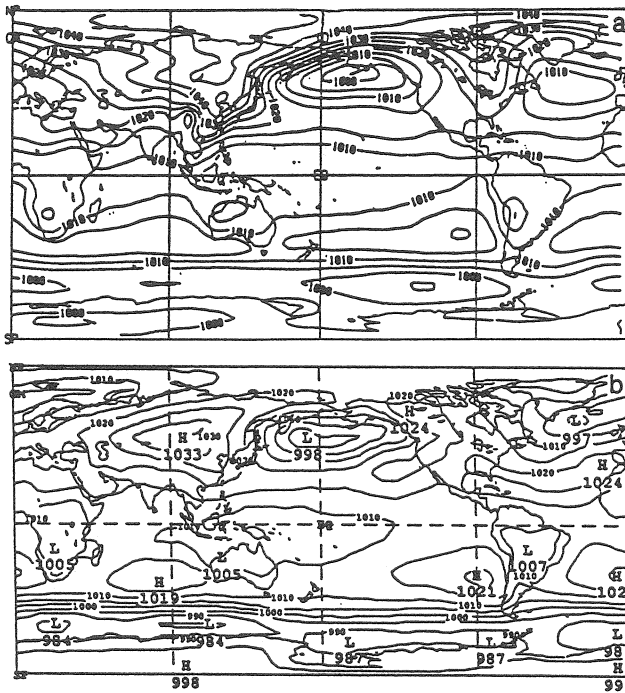


Figure 1 In the upper and lower panels respectively are shown the computed and observed surface pressure distributions for January.

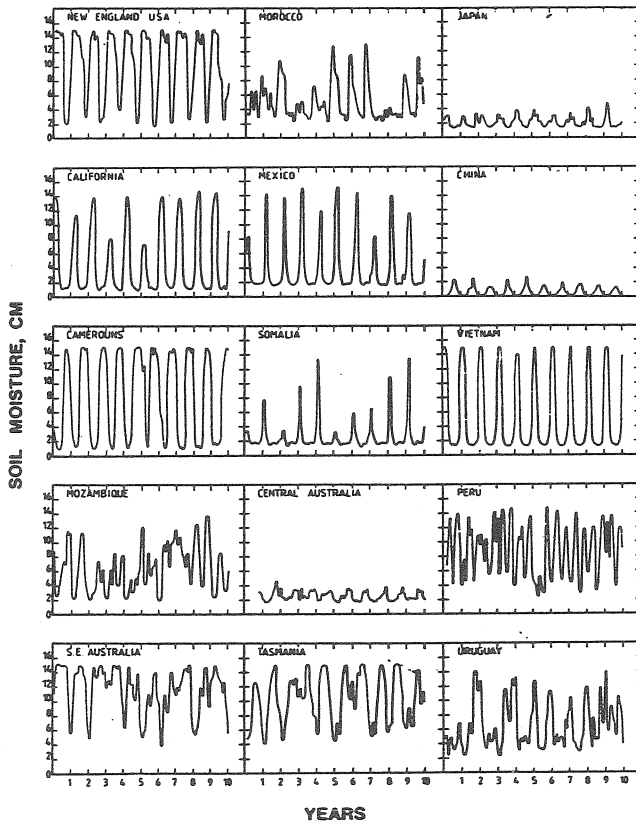


Figure 2 The interannual variation of soil moisture for selected points from a 10-year model run.

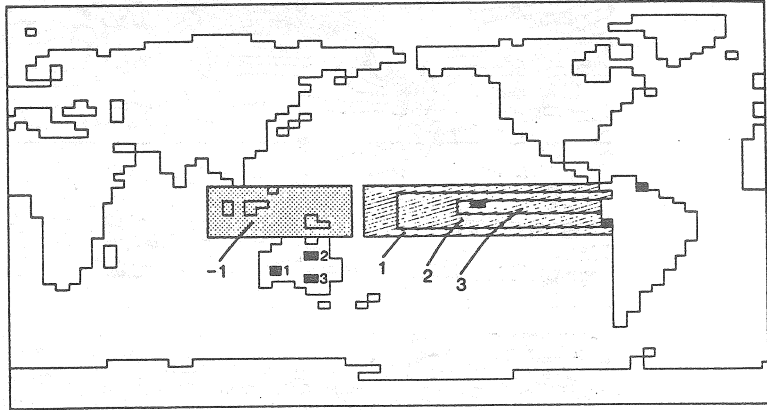


Figure 3 Sea surface temperature anomalies used in the experiments. Experiment D used only the warm anomaly (hatched), experiment E the warm and cold anomaly (stippled). The amplitudes of the anomalies in degrees Celsius are indicated. The black rectangles are model gridpoints for which results are presented in Fig.4.

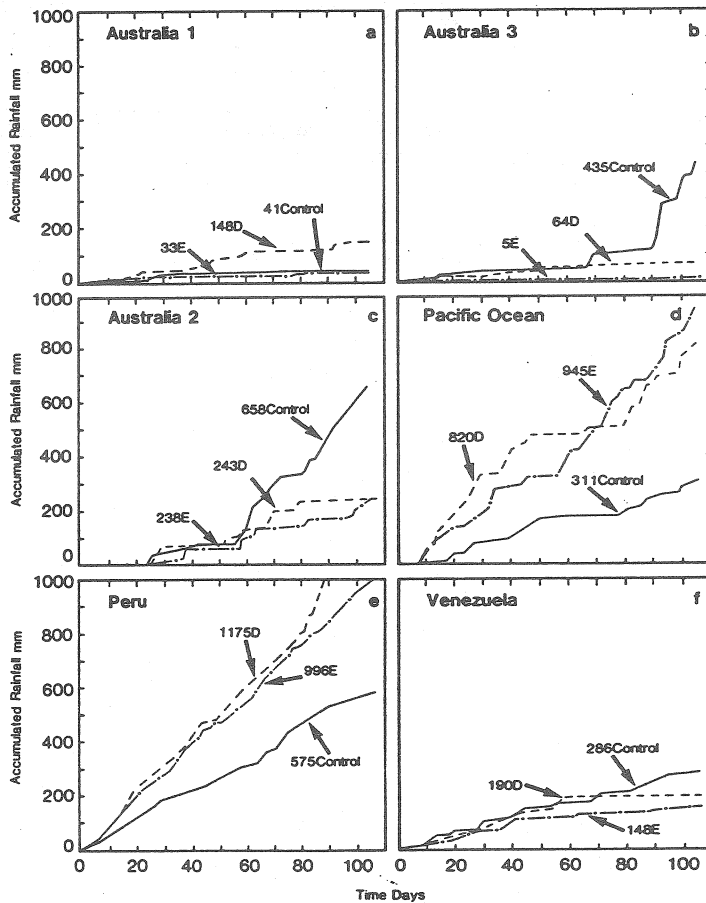


Figure 4 Time series for the control, D and E runs for the 100 days of the experiment. See Fig.3 for location of gridpoints used in this figure. The 100-day rainfall totals in millimetres for each run are shown in the individual panels.

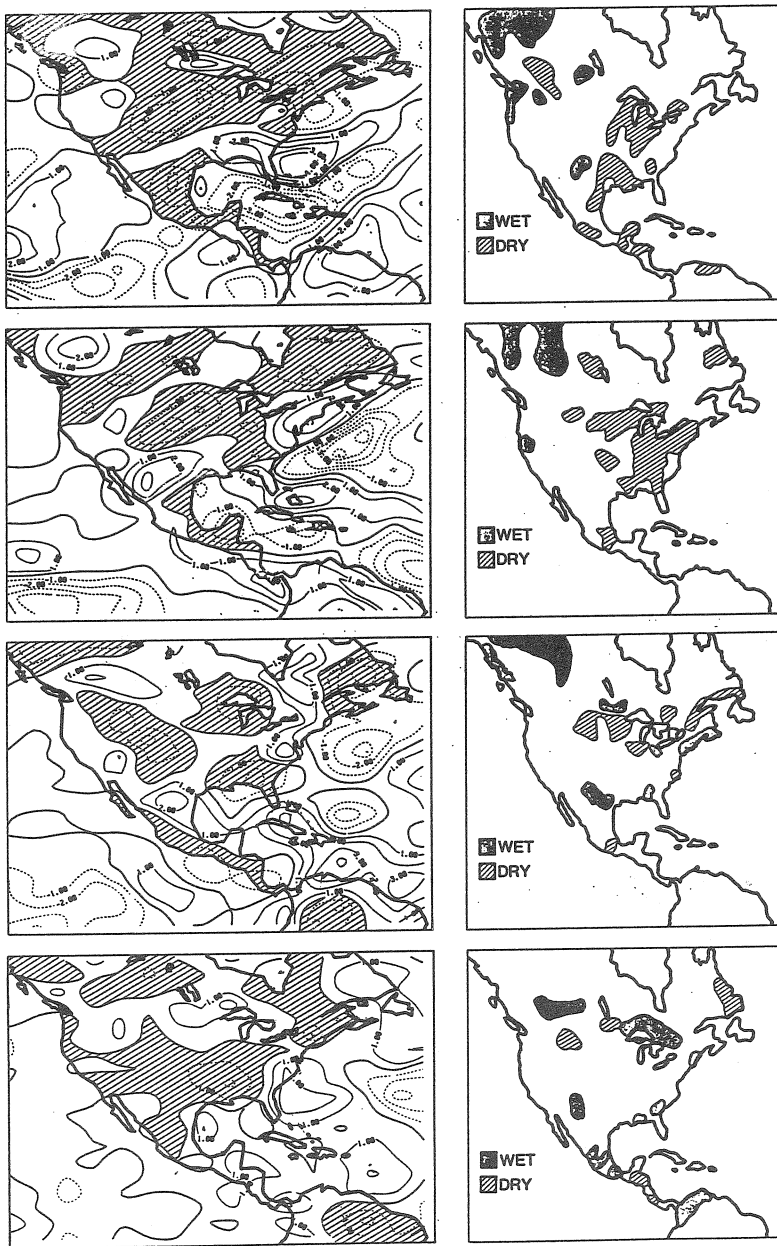


Figure 5 Monthly mean rainfall anomalies over North America from May to August. The left hand panels are computed rainfall changes resulting from including observed SST anomalies for the individual months for the Pacific Ocean. Hatched areas are regions of rainfall reduction. The right hand panels show extreme observed rainfall anomalies for 1988, within the wettest or driest 10% of climatological occurrences.

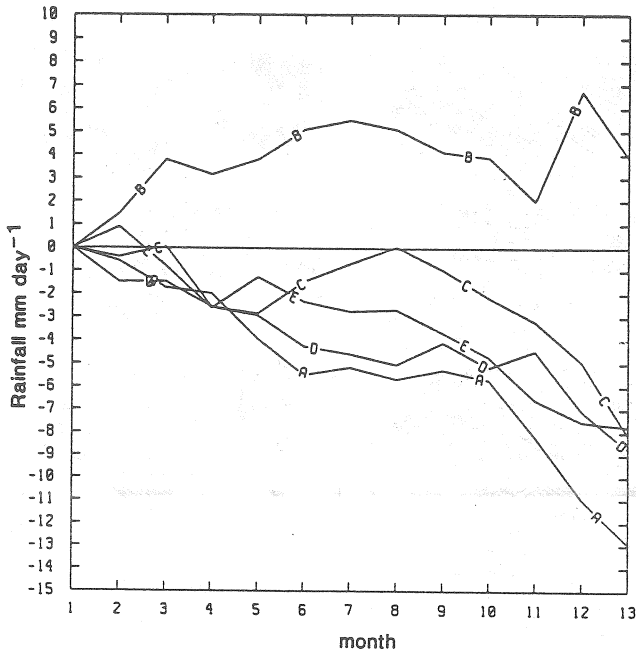


Figure 6 Time series of rainfall changes for a point in northern Australia associated with an idealised El Niño SST anomaly. Results from 5 experiments all using the same anomaly pattern are shown, with each experiment starting from a different year of a model control run.

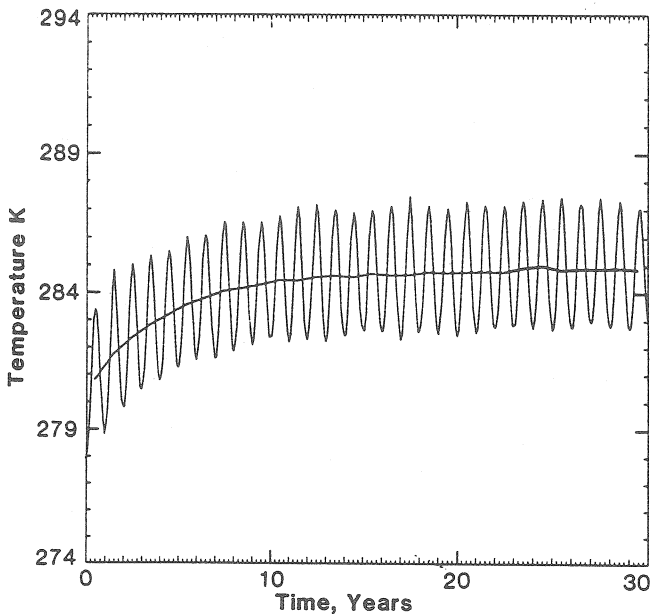


Figure 7 The global mean temperature change at 900 mb in the atmosphere resulting from an instantaneous doubling of the CO_2 amount in the model at year 0. The oscillating curve shows the seasonal variation, the other curve the time-smoothed temperature evolution. A global mean warming of 4 Celsius was obtained.

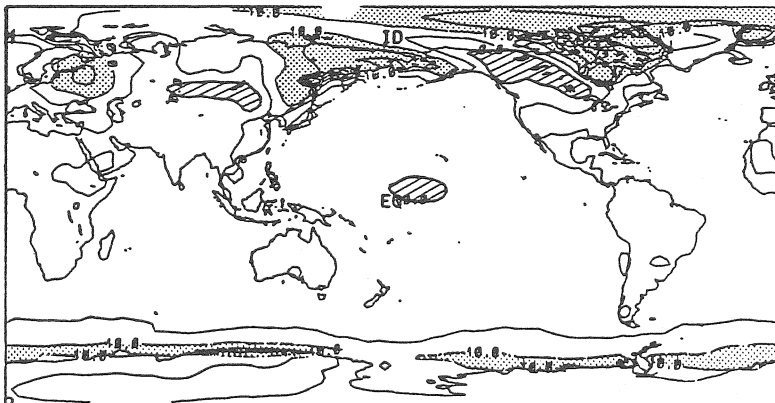


Figure 8 The temperature changes from model climatology of a $1 \times \text{CO}_2$ run for an individual February of a $2 \times \text{CO}_2$ run. Hatched areas are regions with coolings. Stippled areas have warmings greater than 10 Celsius.

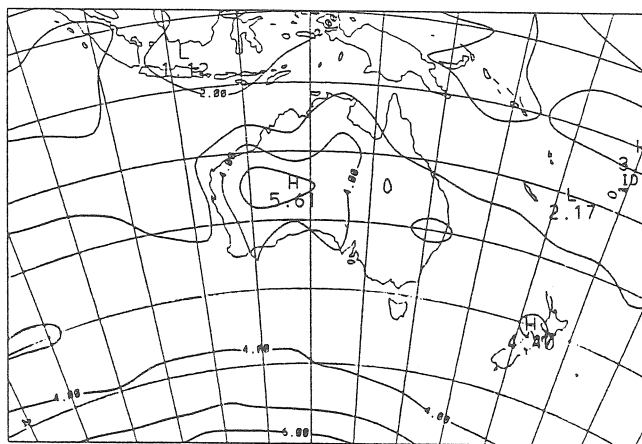


Figure 9 The temperature increases in degrees Celsius over the Australian region for January conditions. Results shown are averaged over a 10-year run.

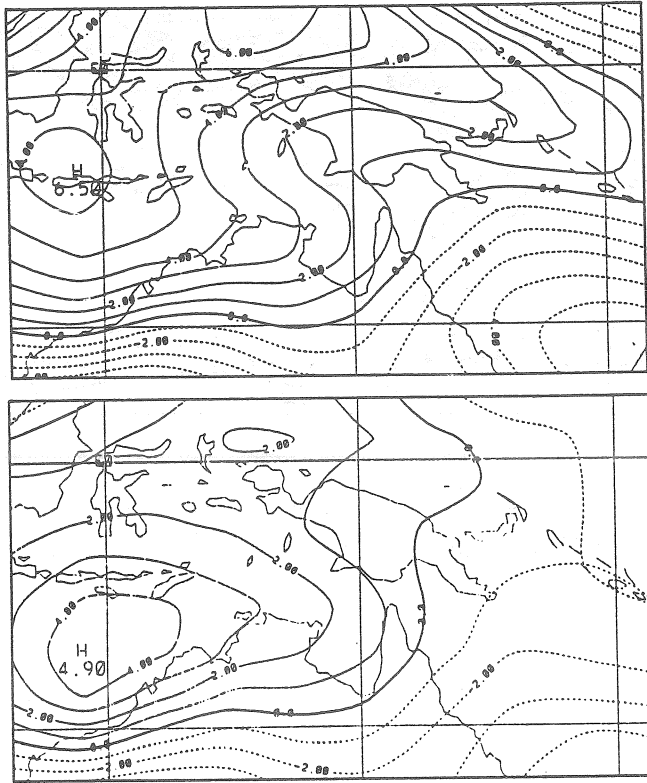


Figure 10 Model generated zonal wind distributions at 900 mb for $2 \times \text{CO}_2$ and $1 \times \text{CO}_2$ runs are shown in the top and bottom panels respectively for the northern Australia region for January. Full lines are west winds, dashed lines east winds, speeds are given in metres per second.

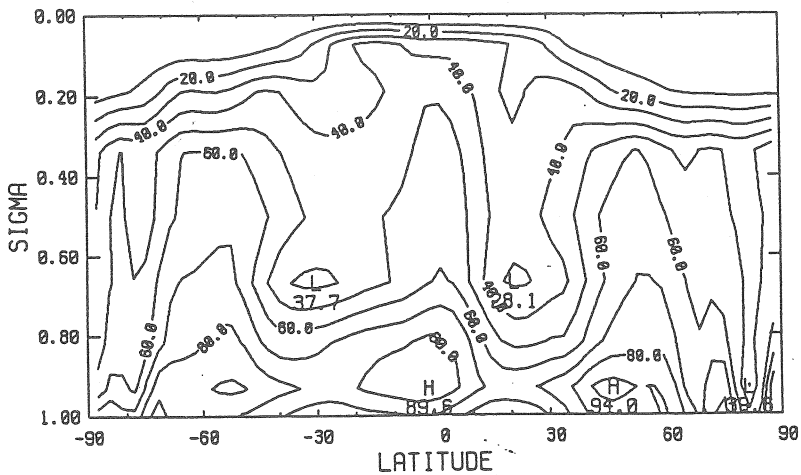


Figure 11 The zonal mean relative humidity computed with the 9-level model for fixed January conditions. Values are in percent.

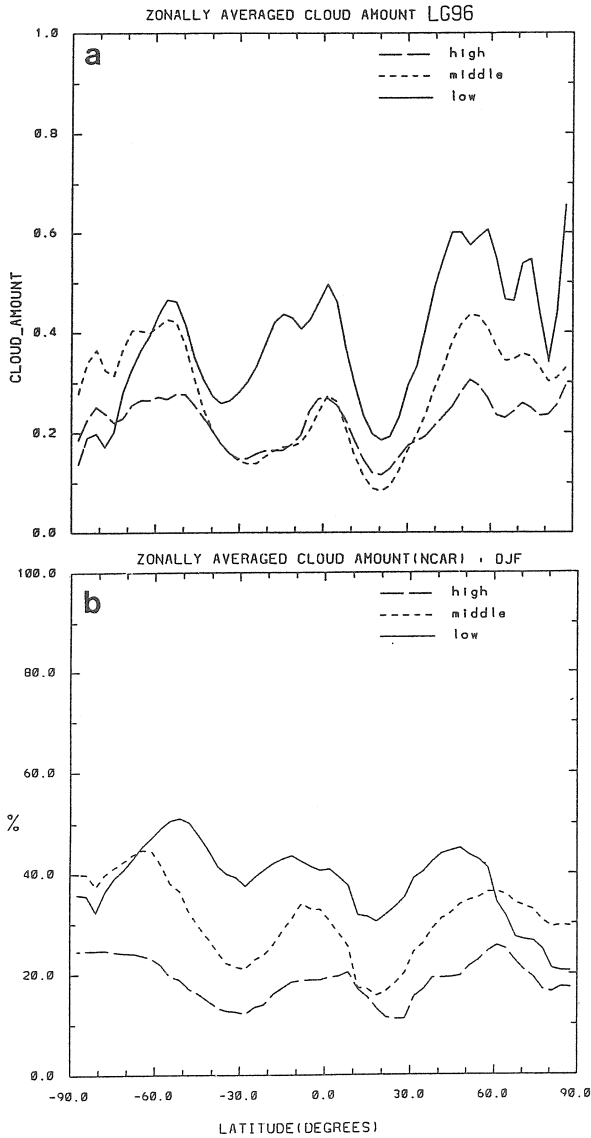


Figure 12 Computed zonally averaged cloud for fixed January conditions is shown in the top panel. Observed cloud in the lower panel averaged over December, January and February.

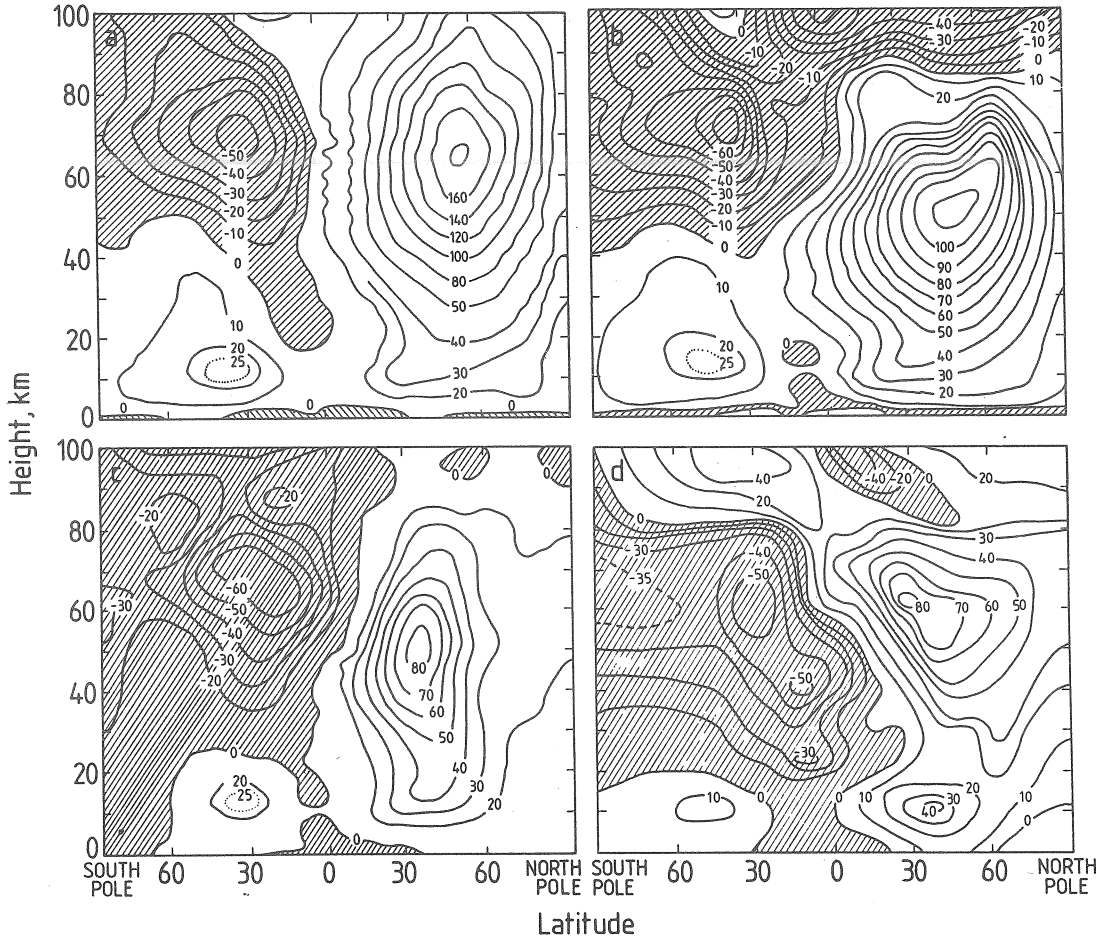


Figure 13 Computed zonally averaged wind for fixed January conditions for various stages of the 54-layer model development is shown in panels (a), (b) and (c). Observations are given in panel (d). Hatched areas are regions with east winds. Units: m s^{-1} .

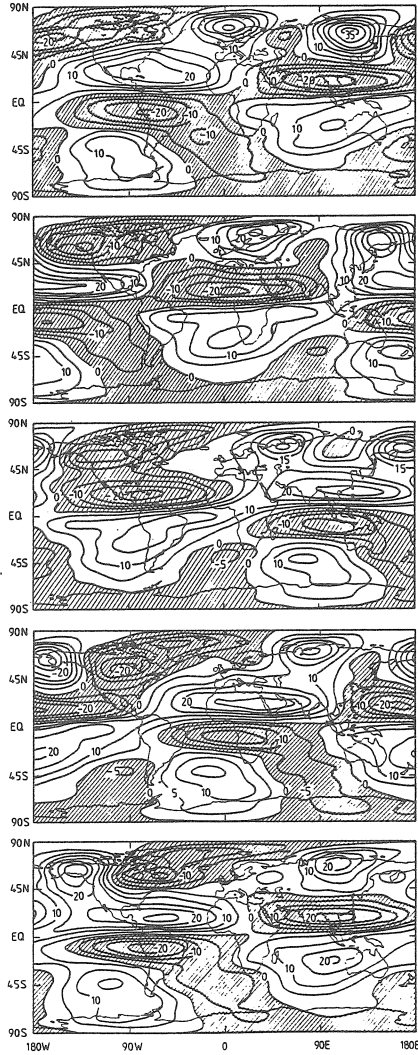


Figure 14 Geographical distributions of the computed meridional wind at 77.5 km are shown at 6-hourly intervals. Hatched areas are regions with southward winds. Units: m s^{-1} .

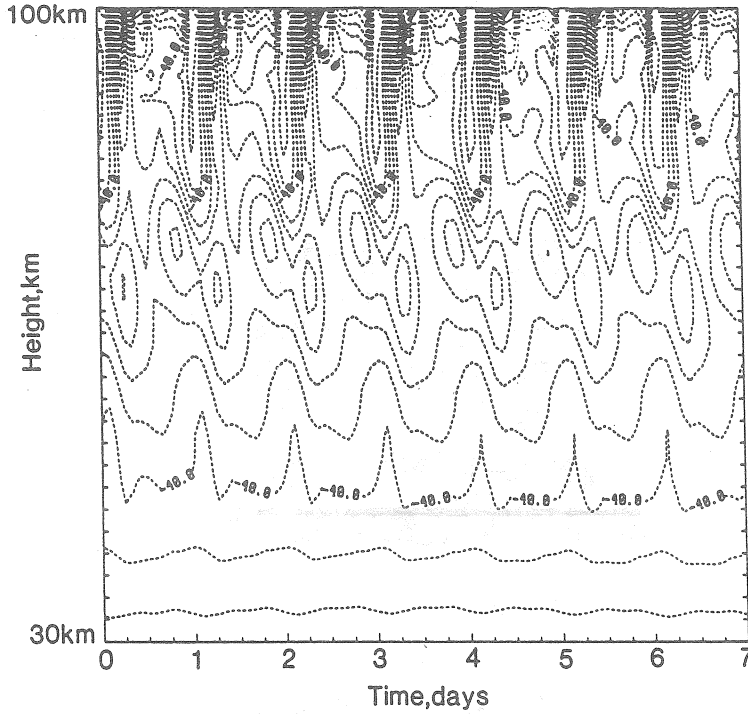


Figure 15 Time-height distribution of the zonal wind for a model gridpoint in South Australia. Units: m s^{-1} .

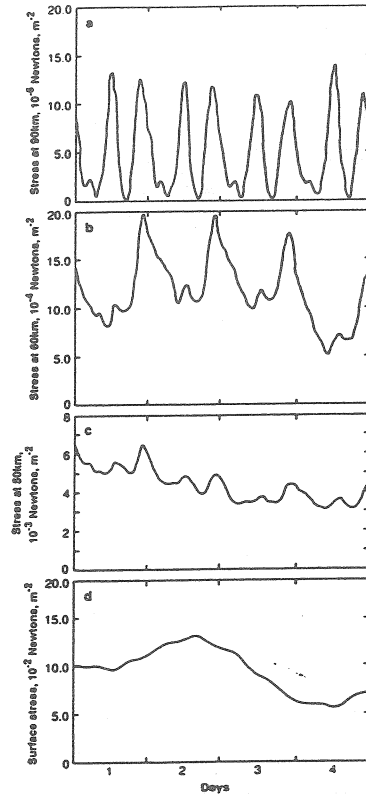


Figure 16 Variation of stress produced by internal gravity waves as a function of time for selected heights.